High quality refinable G-splines for locally quad-dominant meshes with T-gons

K. Karčiauskas[a] & J. Peters[b]

[a] Vilnius University, Lithuania   [b] University of Florida, USA

Abstract

Polyhedral modeling and re-meshing algorithms use T-junctions to add or remove feature lines in a quadrilateral mesh. In many ways this is akin to adaptive knot insertion in a tensor-product spline, but differs in that the designer or meshing algorithm does not necessarily protect the consistent combinatorial structure that is required to interpret the resulting quad-dominant mesh as the control net of a hierarchical spline – and so associate a smooth surface with the mesh as in the popular tensor-product spline paradigm. While G-splines for multi-sided holes or generalized subdivision can, in principle, convert quad-dominant meshes with T-junctions into smooth surfaces, they do not preserve the two preferred directions and so cause visible shape artifacts.

Only recently have n-gons with T-junctions (T-gons) in unstructured quad-dominant meshes been recognized as a distinct challenge for generalized splines. This paper makes precise the notion of locally quad-dominant *mesh as quad-meshes including τ-nets, i.e. T-gons surrounded by quads; and presents the first high-quality G-spline construction that can use τ-nets as control nets for spline surfaces suitable, e.g., for automobile outer surfaces. Remarkably, T-gons can be neighbors, separated by only one quad, both of T-gons and of points where many quads meet. A τ-net surface cap consists of 16 polynomial pieces of degree (3,5) and is refinable in a way that is consistent with the surrounding surface. An alternative, everywhere bi-3 cap is not formally smooth, but achieves the same high-quality highlight line distribution.*

1. Introduction

When working from a polyhedral model, artists can create new degrees of freedom by inserting additional quad strips. Where two quads on one side meet one facet on the other, the meshlines form a 'T' and the polygonal facet is therefore called a T-gon: Fig. 1b and Fig. 1c show T-gons with one and two T-junctions respectively. T-gons also prominently feature in quad-dominant remeshing (see e.g. [ACSD*03, RLL*06, LKH08, JTPSH15, STJ*17]) where they allow to side-step the otherwise stringent global quad-meshing constraints (see e.g. [KNP07, ZSW10, BCE*13, PBJW14, MPZ14]). Also popular in this context are (isolated) triangles that merge and so reduce the number of quad-strips, see Fig. 1a. Since other multi-sided configurations can be modeled by $n \neq 4$ quads meeting at an irregular node, a disciplined design or re-meshing algorithm has no need for additional non-quad facets.

Given the success of tensor-product splines as an intuitive bridge between the world of meshes and the continuous representations preferred for geometric modeling and engineering analysis, ideally the meshes of polyhedral models with T-gons can immediately serve as control nets of (generalized) splines, i.e. their vertices act as coefficients of linear combinations of splines that model appealing surfaces. Hierarchical and T-splines such as [Kra98, SZBN03, GJS12, WZLH17] need to carefully coordinate knot intervals to admit meshes with T-gons as control nets. For
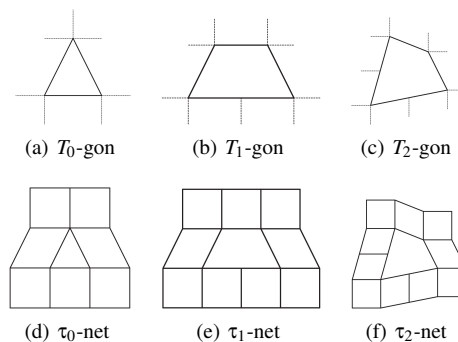

Figure 1: *T-gons and τ-configurations. The subscript counts the number of T-junctions.*

(a) T_0-gon   (b) T_1-gon   (c) T_2-gon

(d) τ_0-net   (e) τ_1-net   (f) τ_2-net

many meshes, e.g. Fig. 2 bottom, a globally consistent choice of intervals is impossible.

[KPP17] introduced G-splines for T_1- and T_2-gons. The construction requires T-gons to be isolated by at least two layers of quadrilaterals, and so forces careful placement of T-gons and irregular points. As Section 5 demonstrates, the resulting surfaces are not quite good enough to serve as automobile outer surfaces.

The new construction yields both high-end surface quality and locality. It requires T-gons to be enclosed by only one layer of quads, whose outer vertices may be *irregular*, i.e. have more or
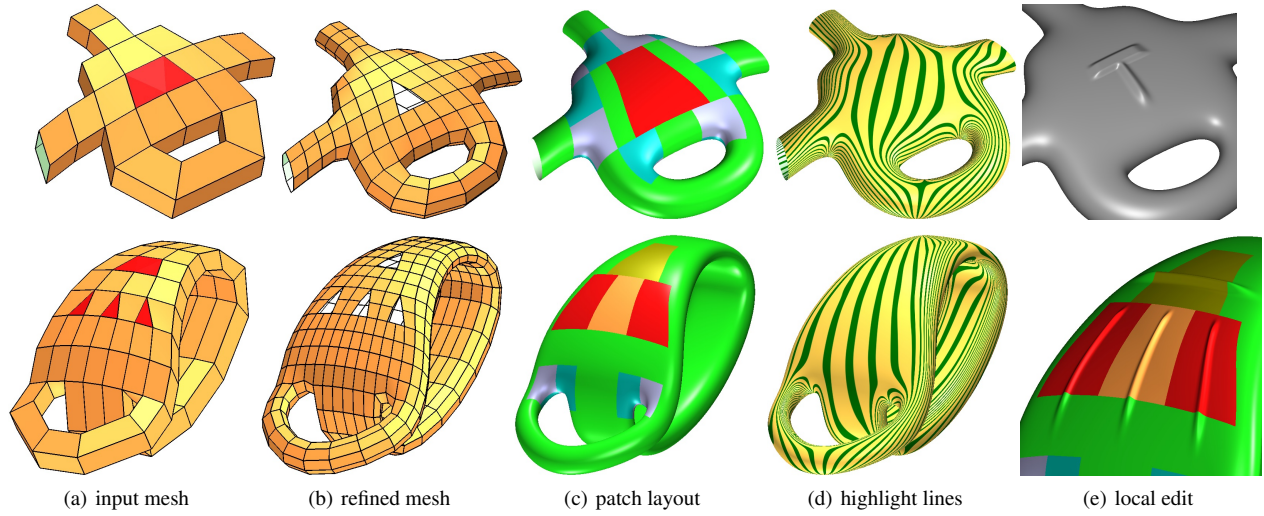
Figure 2: *Using τ-nets as control nets. (a) Mesh with T-gons and irregular nodes of valences* 3 *and* 5 *(covered by [KP15]). (b) Preprocessing: since almost all sub-nets in (a) are not regular, the input mesh is refined everywhere. (c) Patch layout: regular bi-3 patches; τ-spline surface (also orange and yellow where they are close together) and multi-sided caps (grey or blue). (d) highlight lines according to [BC94] should be uniformly spaced where there are no intended features. (e) Using* refinability *to create localized features.*

fewer than four neighbors, or can belong to another T-gon. The key advantages of the new spline over the prior state-of-the art exemplified by [KPP17] are:

- $τ_0$-configurations are covered (see Fig. 1a);
- τ-nets can be placed in close proximity to each other and to irregular nodes (see Fig. 2);
- the highlight line distribution is superior, suitable for automobile outer surfaces;
- the construction can be nestedly refined for engineering analysis or to add geometric detail (see Fig. 2e).

Remarkably, the constructions for $τ_0$ and for $τ_1$ configurations are *unified* into one, reducing the implementation overhead. The unified construction consists of 16 patches of degree $(3,5)$ and is compatible and complements high-quality constructions for multisided, star-like configurations and $τ_2$-nets (see Appendix). Fig. 2 shows examples of such combined modeling where τ-nets are placed in close proximity to each other and to irregular nodes.

Spline covers for τ-configurations are distinct from multi-sided configurations in that they must preserve the two preferred directions, along and across the T-lines. In reference to the layout in Fig. 1, for $τ_0$ and $τ_1$ configurations, we will refer to them as 'vertical' (where mesh density changes) and 'horizontal' (where the flow and density are not to be perturbed). The key is to view τ-surfaces as the result of merging second-order Hermite data from two (virtual, overlapping) tensor-product splines. From this vantage point, we can explain (warn)

- why direction-agnostic constructions such as subdivision surfaces fail to produce good shape; and
- where not to place T-junctions in a quad-dominant mesh.

Overview After introducing T-gons, τ-nets, and several technical construction tools, Section 3 defines the unified construction for

$τ_0$- and $τ_1$-configurations. Section 4 introduces variants of this construction that are curvature continuous, quantifiably almost curvature continuous, respectively everywhere bi-3 with normal discontinuities below an accepted industry threshold. Section 5 discusses choices and limitations and compares to alternative constructions.

1.1. Related constructions

T_0 configurations frequently arise in remeshing and in polyhedral, e.g. automobile, design sketches. T-splines and hierarchical splines do not consider T_0 configurations. [KSD14] uses T_0-gons to create creases or reduce continuity by doubling up knot lines that can be ended in T-junctions.

To leverage hierarchical splines [Kra98], T-splines [SZBN03, GJS12, WZLH17] or [KSD14], for smoothing a given quad-dominant mesh, one needs to discover and assign knot spacings. Also Dyadic Subdivision [KBZ15] relies on a knot structure. While more flexible, the half-edge-reinterpretation of knot spacings in [CZ17] still requires global coordination: arbitrary T-meshes are ruled out and a consistent label assignment may not exist, e.g. for the example of Fig. 2 of [KPP17]. In [CZ17] extraordinary points need to be isolated by three regular rings. The construction in [WZLH17] combines T-splines with a (2-ring-)isolated construction for star configurations. The focus of the construction [KP19b] is refinability. It generalizes (curvature dis-continuous) bi-2 splines, has a dual structure (i.e. the patch vertices are roughly averages of four control points) and a corresponding multi-sided construction of low degree. However, it has a distinctly lower surface quality, including sharply turning highlight lines, than the essentially curvature continuous, primal constructions of this paper that generalize C^2 bi-3 splines. Similarly, the focus of the construction in [KP19a] is to localize the construction in [KPP17]. The proposed algorithm achieves both locality and

refinability with a unified construction, but focuses on superior shape.

2. Setup and Tools

This section defines the setup and tools for the algorithm in Section 3. After defining T-gons, τ-nets and the piecewise polynomial surface representation, Section 2.3 presents the reparameterization and Section 2.4 explicit coefficient formulas for smoothly changing quad-strip densities near T-gons.

2.1. T-gons and τ-nets

Fig. 1 shows the practically relevant τ configurations consisting of one non-quadrilateral facet, called *T-gon*, surrounded by quadrilateral facets (quads). In contrast to the larger footprint T-nets defined in [KPP17], a τ-net has no restrictions on the nodes that do not belong to the T-gon: all outer nodes in Fig. 1 may be *irregular*, i.e. have more or fewer than four neighbors, or can belong to another T-gon. The (minimal) separation due to the single frame of quads is essential for getting high quality surfaces. Meshes consisting of quads and τ-nets are called *locally quad-dominant*, a term inspired by the observation that less separation, e.g. two non-quad facets sharing a vertex, no longer gives the impression of 'quad-dominance' in the local neighborhood.

Connecting a T-junction to one of the two opposite vertices of the T_1-gon converts the τ_1 configuration to a τ_0 configuration but destroys symmetries in the model. But adding to a T_3-net

Figure 3: T_3-net

two edges (marked red in Fig. 3) results in a mesh with a τ_0-subnet. And, despite its smaller footprint, the τ_0 construction developed in this paper is of higher quality than the T_3 construction in [KPP17].
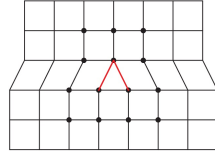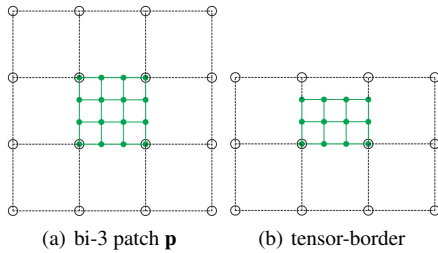

Figure 4: *Bi-3 B-to-BB conversion. Circles $\circ$ mark B-spline control points, solid disks $\bullet$ mark BB-coefficients.*

2.2. BB-form and tensor-borders

The generalized spline surfaces will be a collection of tensor-product patches in Bernstein-Bézier form (BB-form; see e.g. [Far88]) of bi-degree (d_1, d_2) (short bi-d if $d_1 = d_2 = d$):

$$\mathbf{p}(u,v) := \sum_{k=0}^{d_1} \sum_{\ell=0}^{d_2} \mathbf{p}_{k\ell} B_k^{d_1}(u) B_\ell^{d_2}(v), \quad (u,v) \in [0..1]^2,$$

where $B_i^d(t) := \binom{d}{i}(1-t)^{d-i}t^i$ are the Bernstein polynomials of degree d and $\mathbf{p}_{ij}$ are the BB-coefficients. Connecting $\mathbf{p}_{ij}$ to $\mathbf{p}_{i+1,j}$

and $\mathbf{p}_{i,j+1}$ wherever possible yields the *BB-net*. A useful operation on polynomials in BB-form is to split them into two pieces, say a left half and a right half, by the well-known *de Casteljau algorithm* [Far88].

The vertices of any 4×4 sub-grid in the mesh can be interpreted as the control net of a uniform bi-3 B-spline [dB78], the grey net in Fig. 4a. The *B-to-BB conversion*, i.e. expressing this spline in bi-3 BB-form, yields the green BB-net in Fig. 4a. A partial conversion from a partial mesh yields a sub-net of the BB-net. A sub-net defining position, first and second derivatives across an edge Fig. 4b is called a *tensor-border*.

2.3. Reparameterizations

The splines for T-junctions are based on the concept of geometric-continuity, see e.g. [DeR90]. Patches $\mathbf{p}$ and $\mathbf{q}$ that share an edge parameterized by $(u, 0 = v)$ are G^1 connected if their derivatives agree after a change of variables (reparameterization). We denote the first-order and second-order expansions (jets) of $\mathbf{p}(u,v)$ with respect to v by

$$\mathbf{j}^1\mathbf{p}(u,v) := \mathbf{p}(u,0) + \partial_v\mathbf{p}(u,0)v, \tag{1}$$

$$\mathbf{j}^2\mathbf{p}(u,v) := \mathbf{p}(u,0) + \partial_v\mathbf{p}(u,0)v + \frac{1}{2}\partial_{vv}\mathbf{p}(u,0)v^2. \tag{2}$$

In this paper $\mathbf{q} := \mathbf{p} \circ \rho$ where $\mathbf{p}$ has degree bi-3 and the reparameterization $\rho(u,v) := (u, a(u)v)$ has $a(u)$ a polynomial of degree $d = 2$ or $d = 3$ with coefficient vector $\mathbf{a} := [a_0, \ldots, a_d]$. Differentiation of $\mathbf{j}^1\mathbf{p}$ and $\mathbf{j}^2\mathbf{p}$ after composition with ρ implies that $\mathbf{j}^1\mathbf{q}$ is of u-degree $3 + d$, and $\mathbf{j}^2\mathbf{q}$ of u-degree $3 + 2d$. In order not to exceed degree 5 when using a quadratic $a(u)$ in the main construction, $\mathbf{j}^2\mathbf{q}$ is approximated as follows (see Fig. 5).
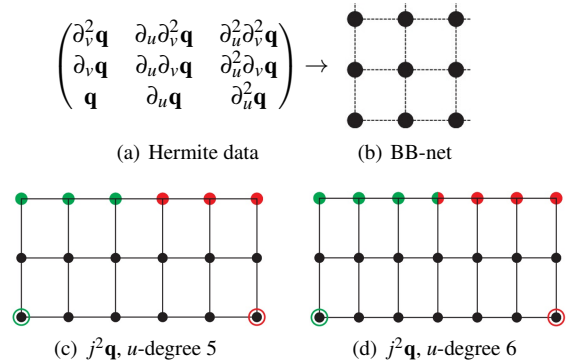

Figure 5: *(a) Second-order Hermite data in partial derivatives form is converted to (b) BB-form. (c) $j^2\mathbf{q}$ of degree 5. (d) $j^2\mathbf{q}$ of degree 4.*

At parameter values $u = 0, 1$ (end-points marked $\circ$ and $\circ$ in Fig. 5c), the second-order Hermite data displayed in Fig. 5a is collected as 3×3 BB-coefficients Fig. 5b and joined to form a BB-presentation of degree $(5, 3)$, displayed Fig. 5c. We denote this approximation of $\mathbf{j}^2\mathbf{q}$ by $j^2\mathbf{q}$. Note that the BB-coefficients marked as black bullets (lower two layers) represent $\mathbf{j}^1\mathbf{q}$ exactly and their bottom layer represents the boundary cubic curve in degree-raised

form. When ρ is linear (as in some parts of the main construction) the second-order expansions are of degree 5 and the conversion represents $\mathbf{j}^2\mathbf{q}$ exactly.

Analogously, in order for $\mathbf{j}^2\mathbf{q}$ not to exceed degree 6 when $a(u)$ is of degree 3, we collect at $u = 0, 1$ the Hermite data

$$
\begin{pmatrix}
\partial_v^2\mathbf{q} & \partial_u\partial_v^2\mathbf{q} & \partial_u^2\partial_v^2\mathbf{q} & \partial_u^3\partial_v^2\mathbf{q} \\
\partial_v\mathbf{q} & \partial_u\partial_v\mathbf{q} & \partial_u^2\partial_v\mathbf{q} & \partial_u^3\partial_v\mathbf{q} \\
\mathbf{q} & \partial_u\mathbf{q} & \partial_u^2\mathbf{q} & \partial_u^3\mathbf{q}
\end{pmatrix}
$$

in degree $(6,3)$ form and average BB-coefficients of the column where the two 4×3 arrangements overlap, see Fig. 5d. This approximation of $\mathbf{j}^2\mathbf{q}$ is also denoted by $j^2\mathbf{q}$ since the context makes the meaning unambiguous. Since $\mathbf{j}^1\mathbf{q}$ is of degree 6, the overlapping black bullets coincide and all black bullets represent $\mathbf{j}^1\mathbf{q}$ exactly. While $j^2\mathbf{q}$ does not always represent $\mathbf{j}^2\mathbf{q}$ exactly, $j^2\mathbf{q}$ picks up shape information crucial for high-quality constructions.

When the expansions $\mathbf{j}^2\mathbf{p}^s$, $s = 1, 2$ are C^2 connected, one can verify by differentiation that $\mathbf{j}^2(\mathbf{p}^s \circ \rho^s)$ are also C^2 connected if $a^s(u)$ are C^2 connected (C^1 connected if so are the $a^s(u)$).

2.4. Technical tools for the unified construction

Here we collect technical results for later reference. The following construction is easy to check.

Lemma 1 (4-piece C^2 formula) Let $\mathbf{b}_i^s$, $i = 0, \ldots, 3$, $s = 0, \ldots, 3$, be the BB-coefficients of four consecutive cubic curves: $\mathbf{b}_0^1 = \mathbf{b}_3^0$, $\mathbf{b}_3^1 = \mathbf{m} = \mathbf{b}_0^2$, $\mathbf{b}_3^2 = \mathbf{b}_0^3$. If

$$
\mathbf{b}_3^0 := \frac{1}{24}\left(-7\mathbf{b}_1^0 + 26\mathbf{b}_2^0 + 6\mathbf{m} - 2\mathbf{b}_1^3 + \mathbf{b}_2^3\right), \tag{3}
$$

$\mathbf{b}_0^3$ is defined by the symmetric formula, and $\mathbf{b}_0^s$, $i = 1, 2$, $s = 1, 2$, are defined by C^2 connection to the outer curves $\mathbf{b}_i^0$, $\mathbf{b}_i^3$, then the inner curves $\mathbf{b}_i^1$, $\mathbf{b}_i^2$ are C^2 connected.
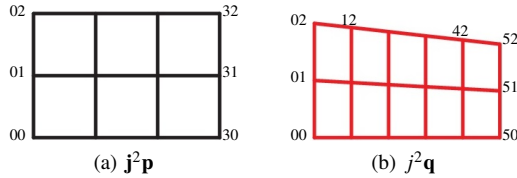

Figure 6: *Labels of (a) input tensor-border $\mathbf{j}^2\mathbf{p}$ (superscripts r, s of γ_{ij}^{rs}) and (b) output tensor-border $j^2\mathbf{q}$ (subscripts i, j of γ_{ij}^{rs}) in Lemma 2.*

Next, we present the formulas for the BB-coefficients of $j^2\mathbf{q} := j^2(\mathbf{p} \circ \rho)$ when $\mathbf{a} := [a_0, a_1, a_2]$. The BB-coefficients of $j^2\mathbf{q}$ are expressed as a weighted sum

$$
\mathbf{q}_{ij} := \sum_{r=0}^{3}\sum_{s=0}^{2}\gamma_{ij}^{rs}\mathbf{p}_{rs}, \quad i = 0, \ldots, 5, \; j = 0, 1, 2, \tag{4}
$$

of the BB-coefficients $\mathbf{p}_{rs}$ of $\mathbf{j}^2\mathbf{p}$. By the choice of ρ, the BB-coefficients $\mathbf{q}_{i0}$, $i = 0, \ldots, 5$ represent the cubic boundary curve with coefficients $\mathbf{p}_{r0}$, $r = 0, \ldots, 3$ in degree-raised form. By symmetry, the weights $\gamma_{5-i,j}^{3-r,s}$, $i = 0, 1, 2$, $j = 1, 2$ are obtained from γ_{ij}^{rs}.

by exchanging a_0 with a_2. Since $\gamma_{i1}^{r2} = 0$, (4) is well-defined once the explicit formulas are given for γ_{i1}^{rs}, $s = 0, 1$, and γ_{i2}^{rs}, $s = 0, 1, 2$ and $i = 0, 1, 2$.

Lemma 2 ($j^2\mathbf{q}$ expansion) Let $i = 0, 1, 2$ and set $\tilde{a}_i := 1 - a_i$, $d_0 := a_0 - 2a_1$, $d_1 := d_0(d_0 + 2a_0)$. For γ_{ij}^{rs} in (4) (see Fig. 6) if $r > i$ then $\gamma_{ij}^{rs} = 0$. Otherwise

$$
\begin{bmatrix}\gamma_{01}^{01} \\ \gamma_{01}^{00}\end{bmatrix} := \begin{bmatrix}a_0 \\ \tilde{a}_0\end{bmatrix}, \quad \begin{bmatrix}\gamma_{11}^{1} \\ \gamma_{11}^{0}\end{bmatrix} := \frac{1}{5}\begin{bmatrix}2a_1 & 3a_0 \\ 2\tilde{a}_1 & 3\tilde{a}_0\end{bmatrix}, \quad \begin{bmatrix}\gamma_{21}^{1} \\ \gamma_{21}^{0}\end{bmatrix} := \frac{1}{10}\begin{bmatrix}a_2 & 6a_1 & 3a_0 \\ \tilde{a}_2 & 6\tilde{a}_1 & 3\tilde{a}_0\end{bmatrix}
$$

$$
\begin{bmatrix}\gamma_{01}^{02} \\ \gamma_{01}^{01} \\ \gamma_{01}^{00}\end{bmatrix} := \begin{bmatrix}a_0^2 \\ 1-(:) \\ \tilde{a}_0^2\end{bmatrix}, \quad \begin{bmatrix}\gamma_{11}^{2} \\ \gamma_{11}^{1} \\ \gamma_{11}^{0}\end{bmatrix} := \frac{1}{5}\begin{bmatrix}-2a_0d_0 & 3a_0^2 \\ 2-(:) & 3-(:) \\ 2\tilde{a}_0(d_0+1) & 3\tilde{a}_0^2\end{bmatrix},
$$

$$
\begin{bmatrix}\gamma_{21}^{2} \\ \gamma_{21}^{1} \\ \gamma_{21}^{0}\end{bmatrix} := \frac{1}{10}\begin{bmatrix}d_1+2a_0a_2 & -6a_0d_0 & 3a_0^2 \\ 1-(:) & 6-(:) & 3-(:) \\ d_1+1-2\tilde{a}_0a_2 & 6\tilde{a}_0(d_0+1) & 3\tilde{a}_0^2\end{bmatrix},
$$

where $(:)$ denotes the sum of top and bottom entries of a corresponding column.

As a consequence of de Casteljau's algorithm we observe the following.

Lemma 3 Consider a curve $h(u)$ with BB-coefficients $h_0, h_1, h_2, \ldots$ over a halved domain: i.e. $\bar{h}(u) := h(\frac{u}{2})$. Then

$$
\bar{h}_0 := 0, \; \bar{h}_1 := \frac{1}{2}h_0 + \frac{1}{2}h_1, \; \bar{h}_2 := \frac{1}{4}h_0 + \frac{1}{2}h_1 + \frac{1}{4}h_2. \tag{5}
$$

3. Splines for τ_0- and τ_1-configurations

In this section, we build a frame of tensor-borders and fill it with a refinable cap. Remarkably, a localized subdivision yields a *common, once-finer control net* for both τ_0- and τ_1-nets (Section 3.1) so that the remaining gap can be filled by a single surface cap construction (Section 3.2). Both the cap and its surrounding mesh are each nestedly refinable (Section 3.3).
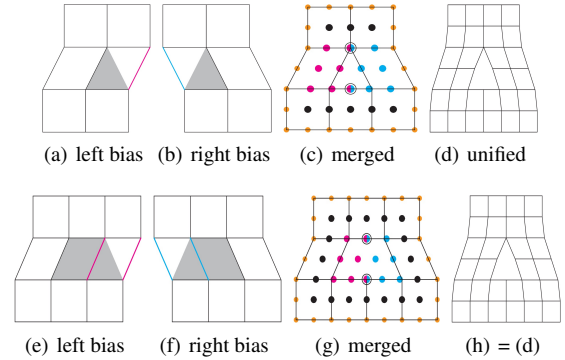

(a) left bias   (b) right bias   (c) merged   (d) unified

(e) left bias   (f) right bias   (g) merged   (h) = (d)

Figure 7: *Unified control net (d)=(h) after refining (top) τ_0 and (bottom) τ_1. (a,b,e,f) biased reconnected subnets; (c,g) merged refinements; (d=h) input (not a BB-net!) for unified construction.*

3.1. Merging regular refinements

Re-meshing with left bias (magenta edges in Fig. 7a,e) and right bias (cyan edges in Fig. 7b,f) yields two biased sub-nets whose regular subdivision defines control points marked as black, magenta

or cyan bullets, are merged (averaged at overlapping locations), see Fig. 7c,g. The outermost orange control points are independently defined by neighboring configurations, i.e. by one of: regular B-spline refinement, the new τ-net rules, extraordinary Catmull-Clark rules, or special boundary rules. Removing its leftmost and right-most control-net layers in Fig. 7g, we get the same mesh connectivity Fig. 7h as in Fig. 7d.
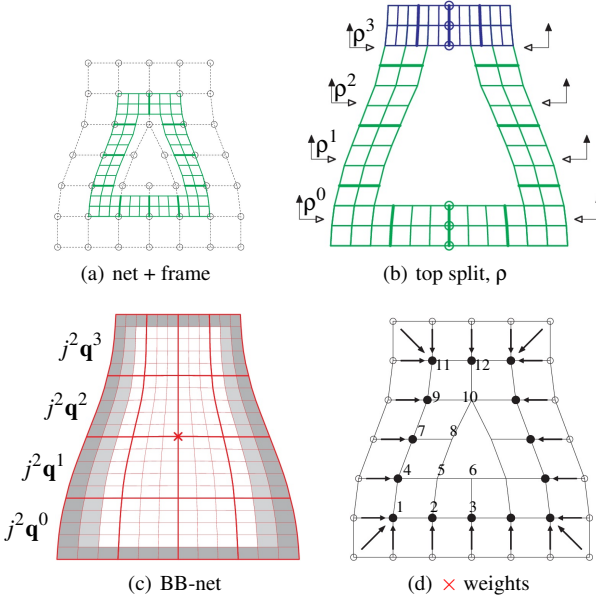

(a) net + frame   (b) top split, ρ

(c) BB-net   (d) × weights

Figure 8: *The unified τ construction. (a) Input net and tensor-border frame. B-to-BB conversion to (b) Top frame split causing the reparameterizations of left (and right) tensor-borders. Since the construction is symmetric with respect to the vertical center line, only a subset of the labels is needed. (c) BB-net structure of the cap of bi-degree* $(3,5)$. *(d) Redistribution of weights for computing* ×.

3.2. The unified construction

The net of Fig. 7d is re-displayed as a mesh of gray circles in Fig. 8a. It serves as the *unified* starting point for both τ_0 and τ_1-constructions in steps (i-v):

- (i) (Fig. 8a) Generate a frame of green tensor-borders by partial B-to-BB conversion of the input net.
- (ii) (Fig. 8b) Split the top tensor-borders uniformly into four (blue in Fig. 8b).
- (iii) (Fig. 8c) Reparameterize the left (and right) tensor-borders with

$$\rho^s(u,v) := (u, a^s(u)v), s = 0, \ldots, 3,$$

$$\mathbf{a}^0 := [1, 1, \tfrac{11}{12}], \quad \mathbf{a}^1 := [\tfrac{11}{12}, \tfrac{10}{12}, \tfrac{9}{12}],$$

$$\mathbf{a}^2 := [\tfrac{9}{12}, \tfrac{8}{12}, \tfrac{7}{12}], \quad \mathbf{a}^3 := [\tfrac{7}{12}, \tfrac{1}{2}, \tfrac{1}{2}].$$

so the resulting first-order expansions are consistent with the top and bottom tensor-borders.

Note that the functions $a^s(u)$ are C^1-connected and $a^1(u)$ and $a^2(u)$ are pieces of a *single linear* function.

Fig. 8c shows the structure of 16 patches of degree 3 in the horizontal and degree 5 in the vertical direction. (As in Section 1, we will repeatedly use the terms *horizontal* and *vertical* in this sense of the underlying standard orientation of Fig. 1.) The dark-gray under-laid parts of the BB-net represent the first-order data of the top and bottom tensor-borders of Fig. 8b in (vertically) degree-raised form, and the now consistent first-order expansions $\mathbf{j}^1\mathbf{q}^s$. The light-gray underlaid BB-net represents the additional coefficients of $j^2\mathbf{q}^s$.

- (iv) The central vertical curve of the cap is constructed by applying the rule (3) (followed by degree-raising) to the top and bottom tensor-border coefficients marked as ○ and ○ in Fig. 8b and the central BB-coefficient marked as × in Fig. 8c.
- (v) The remaining BB-coefficients are set by applying rule (3) horizontally to the left and right $j^2\mathbf{q}$ and the central vertical layer.

The choice of × is key to the quality of the resulting surface. Steps (i)–(v) are first executed with × undetermined, i.e. the 16 patches of the cap are expressed in terms of the unknown ×. Then the functional $F_4 f := \int_0^1 \int_0^1 \sum_{i+j=4, i,j \geq 0} \frac{4!}{i!j!} (\partial_s^i \partial_t^j f(s,t))^2 ds dt$, is summed over all 16 patches and × is chosen to minimize this sum. Then × is a weighted sum of control points of the input net. Since the absolute values of the weights of the outer nodes of the net (circles) are smaller than the inner ones by a factor of 10, they are added to the inner weights (bullets) according to the arrows in Fig. 8d. The weights of the inner nodes are then adjusted to sum to 1 and have 3 digits. The final 12 weights w_i of the inner nodes labeled in Fig. 8d are

| $w_{1\ldots6}$: | 0.018 | −0.019 | 0.001 | −0.019 | −0.063 | 0.331 |
| $w_{7\ldots12}$: | 0.092 | 0.24 | −0.015 | 0.198 | 0.013 | −0.024 |

together with their symmetric counterparts complete the formula × := $\sum w_i \bullet_i$.

The next lemma collects the continuity properties of the construction.

Lemma 4 (cap smoothness) The cap is

- (a) C^2 across the three inner vertical curves;
- (b) C^2 across the central horizontal curve;
- (c) G^2 joined to the middle two left and right pieces of the frame in Fig. 8a.
- (d) C^1 across the remaining internal boundaries and
- (e) G^1/C^1 with the remaining tensor-border frame.

Proof (a) follows from (v). (b,c) Since $a^1(u)$ and $a^2(u)$ are pieces of one linear polynomial, $j^2\mathbf{q}^s = \mathbf{j}^2\mathbf{q}^s$ for $s = 1, 2$; and $j^2\mathbf{q}^1$ joins $j^2\mathbf{q}^2 \, C^2$. By construction step (iv) central curve is C^2. (d,e) hold by explicit construction. □

We will see in the examples that the transitions characterized by (d,e) manifest only slight curvature discontinuities.

3.3. G-refinement

The following refinement has two properties valued in design and in engineering analysis: (α) the refinement is nested, i.e. the refined representation can exactly model the coarser representation; (β) the distribution of degrees of freedom (dofs) within the frame of control points follows a regular pattern and so does the distribution of unconstrained BB-coefficients of the cap. To achieve this
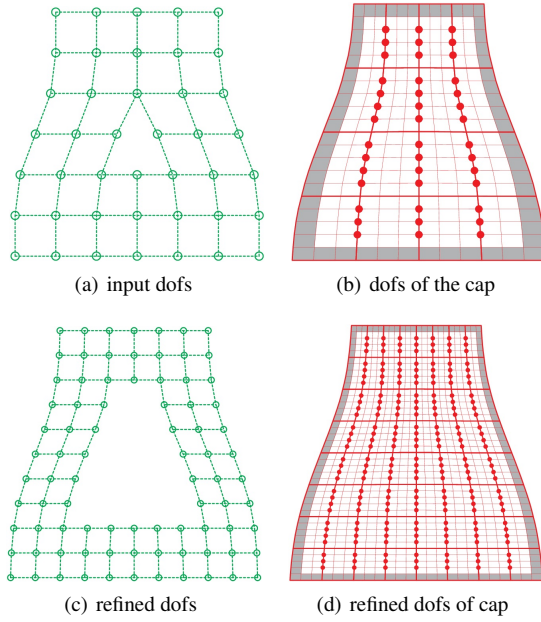
(a) input dofs   (b) dofs of the cap

(c) refined dofs   (d) refined dofs of cap

Figure 9: *Nested refinement. (a) initial degrees of freedom (dofs) of the input mesh ○; (b) initial dofs internal to the cap ●. (c,d) refined dofs.*

regular pattern, after initialization by the unified construction, we adopt a slightly larger space by dropping some second-order (C^2, G^2) constraints. Specifically the control net in Fig. 9a defines only the grey-underlaid BB-net in Fig. 9b but not those marked by ● that represent degrees of freedom of a spline cap that is $C^{2,1}$, namely C^2 in the horizontal but only C^1 in the vertical direction.

Refinement of the interior of the cap then amounts to regular knot insertion into the $C^{2,1}$ spline. Since the top and bottom gray-underlaid BB-nets are C^1 joined to their surrounding bi-3 data, knot insertion also works here and only the degree needs to be taken into account. Finally Lemma 5 establishes the refinement $\mathbf{j}^1\mathbf{q} := \mathbf{j}^1(\mathbf{p} \circ \rho)$ along left and right boundaries with $\rho(u,v) := (u, a(u)v)$. The following is easily verified.

Lemma 5 Partitioning with breakpoints $0, h$ in the v-direction, and d^k in the u-direction, the pieces along the boundary $v = 0$ and between $u = d^k$ and $u = d^{k+1}$ are defined by the maps

$$
\begin{aligned}
\mathbf{p}^k(u,v) &:= \mathbf{p}(d^k(1-u) + d^{k+1}u, hv), \\
\mathbf{q}^k(u,v) &:= \mathbf{q}(d^k(1-u) + d^{k+1}u, hv), \qquad (6) \\
\dot{\rho}^k(u,v) &:= (u, a(d^k(1-u) + d^{k+1}u)v).
\end{aligned}
$$

Then $\mathbf{j}^1\mathbf{q}^k = \mathbf{j}^1(\mathbf{p}^k \circ \dot{\rho}^k)$.

Equations (6) yield the following

Refinement Algorithm

1. Apply knot insertion to the $C^{2,1}$ spline of bi-degree $(3,5)$. (This yields the new degrees of freedom marked ● in Fig. 9d.)

2. Apply standard bi-3 C^2 spline refinement to obtain new dofs displayed in Fig. 9c. (The dofs define the gray-underlaid part of the cap in Fig. 9d.)
3. For horizontal layers with ● apply a standard B-to-BB conversion of cubic C^2 splines with C^1 end-conditions.
4. For the remaining horizontal layers, the BB-coefficients are the averages of their vertical neighbors obtained in 3.

4. Variants of the unified construction

The curvature of the unified degree $(3,5)$ construction is not continuous but well-distributed. The default construction has interesting variants. Increasing the degree to $(3,9)$ yields curvature continuous surfaces (Section 4.1) whose curvature profile is, for all practical purposes replicated by a formally not curvature continuous construction of degree $(3,6)$ (Section 4.2). A

Figure 10: 4×4 *patches of the curvature continuous cap of bi-degree* $(3,9)$; ● *mark dofs.*

third variant of degree $(3,3)$ is formally only C^0 but its normal discontinuities are observed to be below the threshold acceptable in class A automobile outer surfaces (Section 4.3). All variants have the same structure of 16 patches per cap.
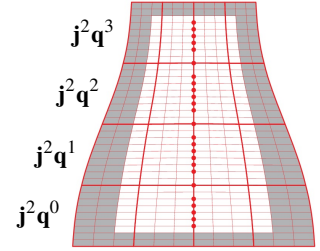
4.1. Curvature continuous cap of bi-degree $(3,9)$

A curvature continuous cap of bi-degree $(3,9)$ is constructed copying steps (i-v) with the following modifications. In (iii), $a^s(u)$ for $\rho^s(u,v) := (u, a^s(u)v)$, $s = 0, \dots, 3$ are cubic functions with coefficients $\mathbf{a} := [a_0, a_1, a_2, a_3]$ defined as

$$
\mathbf{a}^0 := [1, 1, 1, \tfrac{23}{24}], \quad \mathbf{a}^1 := [\tfrac{23}{24}, \tfrac{11}{12}, \tfrac{5}{6}, \tfrac{3}{4}],
$$
$$
\mathbf{a}^2 := [\tfrac{3}{4}, \tfrac{2}{3}, \tfrac{7}{12}, \tfrac{13}{24}], \quad \mathbf{a}^3 := [\tfrac{13}{24}, \tfrac{1}{2}, \tfrac{1}{2}, \tfrac{1}{2}].
$$

In (iv) we degree-raise the curve to 9.

Lemma 6 The $(3,9)$ cap is curvature continuous.

Proof The functions $a^s(u)$ are C^2-connected ($a^1(u)$ and $a^2(u)$ are pieces of one cubic function). The second-order expansions $\mathbf{j}^2\mathbf{q}^s$ (left and right dark-gray underlaid BB-coefficients in Fig. 10) are of degree 9 and consistent with top and bottom tensor-borders (also dark-gray) in degree-raised form; and they are C^2-connected. □

The $(3,9)$ cap refinement along the left and right boundary curves is as in Section 3.3. But, due to higher degree, the refinement of the inner part yields approximately twice the number of C^2 functions (degrees of freedom) for engineering analysis.

The main purpose for introducing the $(3,9)$ cap is to quantify the observed 'almost' curvature continuity of its siblings.

4.2. An 'almost' curvature continuous cap of bi-degree $(3,6)$

A bi-degree $(3,6)$ construction, formally just G^1-joined to the 'left and right' input data is visually indistinguishable from the degree $(3,9)$ construction, both in the highlight lines and in curvature plots. As explained in the second half of Section 2.3, the degree 9 expansions $\mathbf{j}^2\mathbf{q}^s$ are approximated by $j^2\mathbf{q}^s$ of degree $(3,6)$ (left and right gray-underlaid strips in Fig. 11a where light-gray indicates the approximated part). With the central vertical layer presented in degree 6 form, rule (3) is applied in the horizontal direction. The resulting cap is internally C^2, G^1 connected to left and right input data and C^2 connected to top and bottom input data.

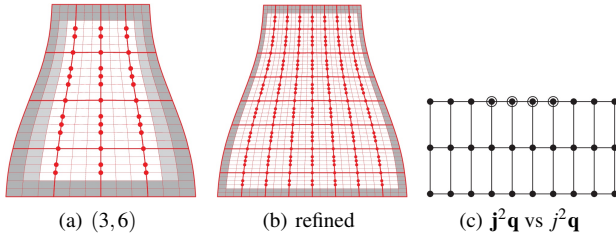|		
(a) $(3,6)$	(b) refined	(c) $\mathbf{j}^2\mathbf{q}$ vs $j^2\mathbf{q}$

Figure 11: *'Almost' curvature continuous cap. (a) Structure of the bi-degree $(3,6)$ cap, (b) once refined. (c) Comparing $\mathbf{j}^2\mathbf{q}$ with $j^2\mathbf{q}$ degree-raised to 9 in the u-direction.*

The ● in Fig. 11a mark inner BB-coefficients of the cap that can serve as dofs for engineering analysis in addition to the subset of light-gray-underlaid BB-coefficients analogous to the bi-degree $(3,5)$ construction in Fig. 9b. After one refinement, the new inner degrees of freedom are again marked by ● in Fig. 11b. The refinement along the left and right bounding curves is as in Section 3.3 but with $j^2\mathbf{q}$ of degree 6.

To quantify 'almost' curvature continuous, we degree-raise $j^2\mathbf{q}$ in the u-direction and compare with $\mathbf{j}^2\mathbf{q}$. The difference is restricted to the circled BB-coefficients in Fig. 11c. For all four pieces $s = 1,..4$, we express both sets of coefficients as affine combinations of the BB-coefficients of input bi-3 $\mathbf{j}^2\mathbf{p}$ with weights w_i^6, respectively w_i^9. Then $\max_i |w_i^6 - w_i^9| < 0.001$. Additionally, we numerically computed for a series of challenging inputs both the Gaussian curvature and the mean curvature, the maximum difference e between exact and 'almost' curvature continuity along the boundary and the difference E between max and min values of the exact curvature. In all cases, we found $\frac{e}{E} < 0.001$. Each refinement of the input data (followed by extension $j^2\mathbf{q}$) further reduces $\max_i |w_i^6 - w_i^9|$ by a factor of 10.

4.3. Bi-3 cap

To further explore the space of τ-surfaces, we reduce the degree $(3,5)$ construction to bi-3 as follows. At the corners where $u = 0, 1$, the Hermite data (see Fig. 12a) of the G^2 expansion according to Lemma 2 is collected as 2×3 arrangements of BB-coefficients in bi-3 form. These are merged to form the BB-net $j^2\mathbf{q}$ of Fig. 12b. (The degree is reduced in the u-direction from 5 in Lemma 2 to 3 by setting the bi-3 coefficients of $\mathbf{q}$ in terms of those of $\hat{\mathbf{q}}$ (of degree 5 in the u-direction) as $\mathbf{q}_{0\ell} := \hat{\mathbf{q}}_{0\ell}$, $\mathbf{q}_{1\ell} := -\frac{2}{3}\hat{\mathbf{q}}_{0\ell} + \frac{5}{3}\hat{\mathbf{q}}_{1\ell}$.) Then

$j^2\mathbf{q}$ represents the boundary curve exactly, as the BB-coefficients marked as ●. Then steps (i-v) of the unified construction (with the central vertical layer kept in degree 3 form) yields the bi-3 cap.

The new bi-3 cap is

- formally only C^0-joined to the left and right input data,
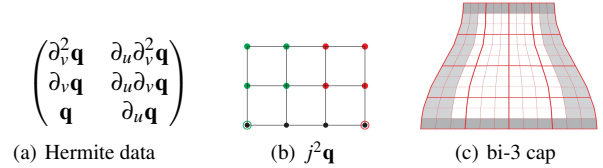- C^1 from top to bottom, and
- C^2 from left to right.

$$\begin{pmatrix} \partial_v^2\mathbf{q} & \partial_u\partial_v^2\mathbf{q} \\ \partial_v\mathbf{q} & \partial_u\partial_v\mathbf{q} \\ \mathbf{q} & \partial_u\mathbf{q} \end{pmatrix}$$

(a) Hermite data	(b) $j^2\mathbf{q}$	(c) bi-3 cap

Figure 12: *Bi-3 construction. (b) $j^2\mathbf{q}$ in bi-3 form. (c) Top and bottom (dark-gray) are C^1-connected to the input tensor-border frame.*

Testing the construction on a sequence of challenging inputs, we found the mismatch of normals to always be less than $0.1°$, acceptable for automobile class A surface design [Aut19].

5. Examples and discussion

This section compares to Catmull-Clark surfaces [CC78], [KPP17], the variants of Section 4 and evaluates interaction with nearby irregular points and mesh creases.
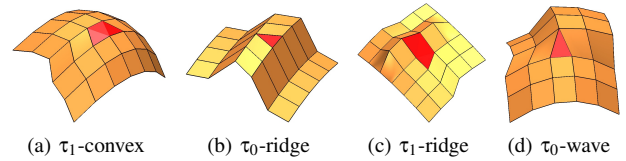

(a) τ_1-convex	(b) τ_0-ridge	(c) τ_1-ridge	(d) τ_0-wave

Figure 13: *Locally quad-dominant test meshes. (a) The nodes of a mesh with T_1-gon lie on an elliptic paraboloid. (b) The ridge top and its two base strips lie on different paraboloids. (c) A copy of (a) with one vertical layer lifted up. (d) A convex mesh with top-right 3×3 sub-net pulled up.*

The test configurations in Fig. 13 place the input mesh on a well-understood basic shape, an elliptic paraboloid in Fig. 13a. Many constructions, for example Catmull-Clark subdivision, produce non-uniform highlight line distributions already for this simple input. As is common in polyhedral design, pieces of basic shapes are merged, Fig. 13b, or sub-meshes displaced, Fig. 13c,d. The test meshes are intentionally small since shortcomings of the spline surface (as opposed to the large scale polyhedral outline) are subtle
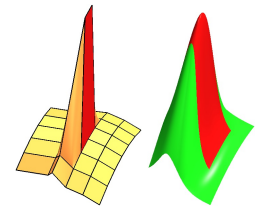

Figure 15: *Bi-3 stress test*

(a) 1 CC step   (b) reprojected   (c) unified layout   (d) bi-3 layout

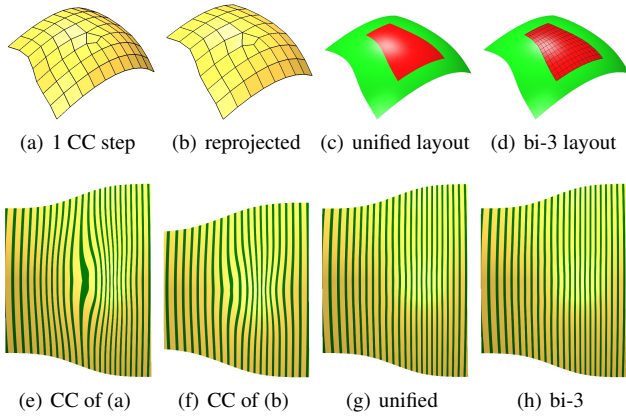(e) CC of (a)   (f) CC of (b)   (g) unified   (h) bi-3

Figure 14: *First three columns: comparison to Catmull-Clark (CC) subdivision. (a) Mesh Fig. 13a after one Catmull-Clark refinement. (b) Subnet of (a) is then projected onto the elliptic paraboloid. (c) The unified construction: regular bi-3 patches, central cap. (d) Bi-3 construction of Section 4.3.*

and local. To be useful for evaluating surface quality, one would anyhow have to zoom in on large meshes.

Fig. 14 demonstrates that Catmull-Clark subdivision is not satisfactory for design with τ_0- and τ_1-nets. The highlight lines emphasize artifacts that are visible already in shaded view. While the highlight line distribution of the unified construction is perfect (Fig. 14g). Fig. 14e shows what Malcolm Sabin aptly named 'first step artifacts', i.e. unwanted waviness. Even re-projecting the relevant part of the refined mesh Fig. 14b onto the initial paraboloid Fig. 14c, to remove the damage of the first step, only improves but does not fix the highlight flaw Fig. 14f. And while 'tuning' can improve the eigenspectrum and limit near the extraordinary point [CADS09, ADS11], the overall shape is typically worse due to first step artifacts. By contrast to the direction-unaware Catmull-Clark subdivision, the unified construction retains the tensor-product bias of the input (this was conveniently used in Fig. 2e to place the 'T'). Fig. 14g,h show visually identical highlight lines for the unified degree $(3,5)$ cap and its bi-3 modification. Indeed for this and other inputs even the curvature shading is nearly indistinguishable. Also the $< 0.1°$ upper bound on the mismatch of the normal continues to hold where the geometry changes extremely fast as in Fig. 15 (the angular deviation of normals is $< 0.068°$).
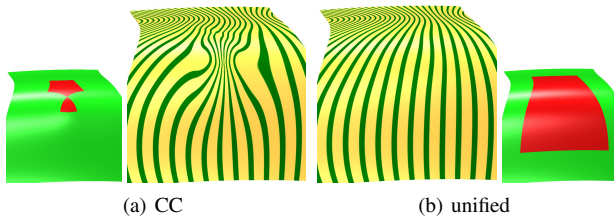

(a) CC   (b) unified

Figure 16: τ_0-*ridge. (a) Catmull-Clark surface and highlight lines. (b) unified construction and highlight lines.*

A further argument against the use of Catmull-Clark subdivision for T-configurations is the outcome in Fig. 16a. Here the central wave is convex. After two steps the bicubic 3- and 5-sided regions become separated (red in Fig. 16a) and the original two-direction layout is forgotten. The resulting poor highlight line distribution contrasts with that of the unified construction Fig. 16b.
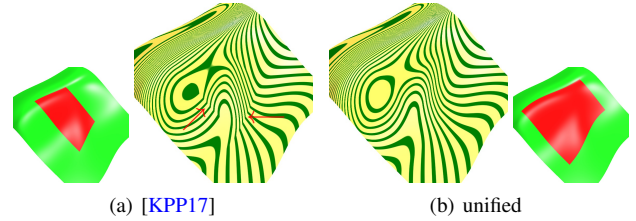

(a) [KPP17]   (b) unified

Figure 17: τ_1-*ridge from Fig. 13: comparing unified to [KPP17].*

Besides its ability to handle much tighter configurations than [KPP17] the unified construction yields visually smoother highlight lines. The arrows $\leftarrow$ in Fig. 17a point to the undesirable sharper turns.
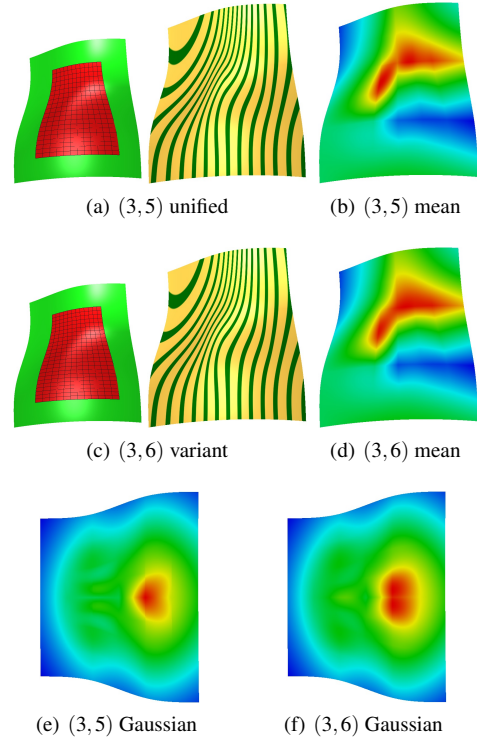

(a) $(3,5)$ unified   (b) $(3,5)$ mean

(c) $(3,6)$ variant   (d) $(3,6)$ mean

(e) $(3,5)$ Gaussian   (f) $(3,6)$ Gaussian

Figure 18: *Comparison of the unified construction and its bi-degree $(3,6)$ variant. Top rows: input mesh Fig. 13d. Bottom row: input mesh Fig. 13a.*

Fig. 18 demonstrates that the degree $(3,5)$ unified construction and its variant of degree $(3,6)$ generate very similar surfaces both visually and comparing their curvatures. Moreover, the degree

(3, 6) surfaces' curvature is near-impossible to distinguish from that of the curvature continuous degree (3, 9) construction.
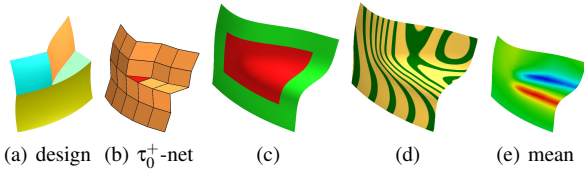

(a) design (b) τ_0^+-net (c) (d) (e) mean

Figure 19: *Natural occurence of a τ_0-net when merging surfaces. (e) mean curvature.*

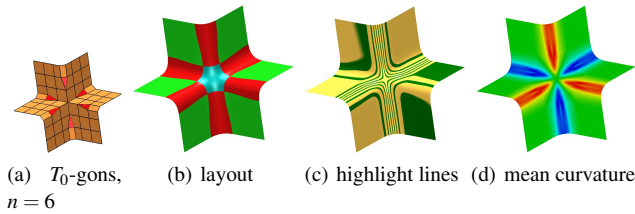(a) T_0-gons, (b) layout (c) highlight lines (d) mean curvature
$n = 6$

Figure 20: *τ-net with high valence vertex: (a) a mesh with six T_0-gons and irregular node of valence 6.*

Fig. 19 shows a designer's sketch, the blending of two 'primary' surfaces. Already Fig. 2 showed T-gons and irregular nodes in close proximity. Fig. 20 re-emphasizes that also higher valences in τ-nets pose no problem.

Where not to place T-junctions. Skilled designers (or good remeshing algorithms) know not to run ridges diagonal to the tensor-product directions since this can give rise to oscillations. In the unified construction two diagonally re-connected tensor-product subnets (see Fig. 21 c,d) are merged. Neither should violate good design practice, even though the merging diminishes the oscillations. Therefore placing the τ-net as in Fig. 21b is asking for trouble. Fig. 21e,f,g show that the unified construction is the most tolerant of the options: the $\rightarrow$ in Fig. 21e points to the flaw in [KPP17] and the direction-agnostic Catmull-Clark subdivision fares worse. By contrast, when a crease is oriented horizontally, as in Fig. 21h,k, the virtual subnets do not introduce a 'camel back' effect of Fig. 21d. (Catmull-Clark subdivision fails also for this input).

Fig. 22 mimics, via a T_1-gon, the insertion of a crease Fig. 22e as is created in (b) by truncated double (triple) knot lines and T_0-gons. Of course the goal for this paper is to smooth out, not create creases.

5.1. Partition of unity and linear independence

For a heterogeneous collection of C^2 B-splines, multi-sided surfaces [KP15] and τ surfaces it is appropriate to define *generating functions* as the collection of polynomial pieces in BB-form obtained from the construction applied to a mesh where one nodal value is one and all others zero. Partition of unity then follows
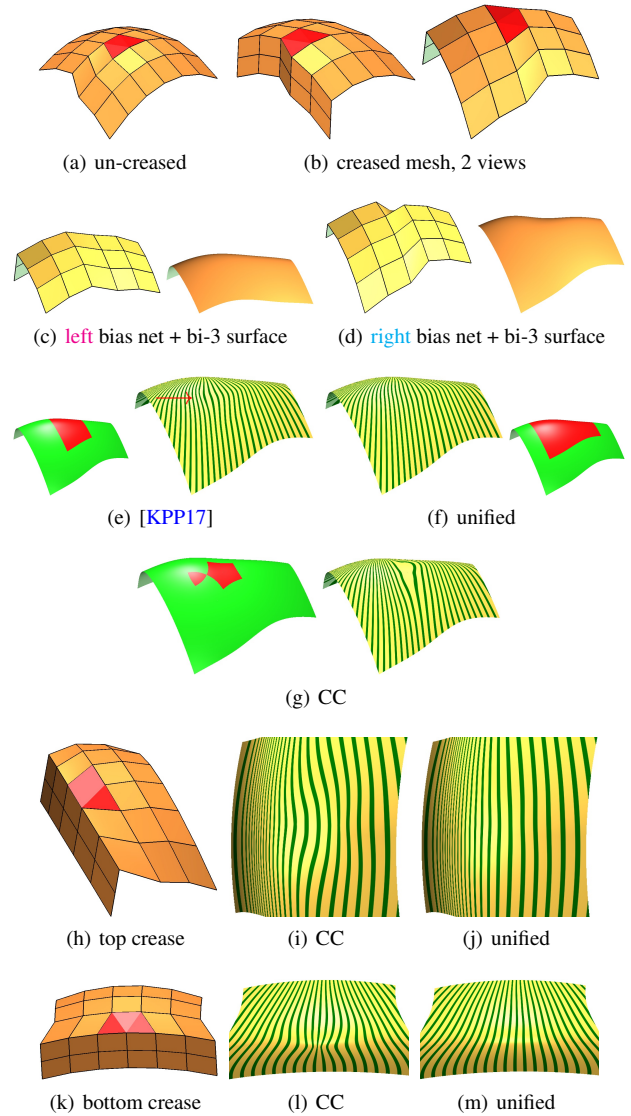

(a) un-creased (b) creased mesh, 2 views

(c) left bias net + bi-3 surface (d) right bias net + bi-3 surface

(e) [KPP17] (f) unified

(g) CC

(h) top crease (i) CC (j) unified

(k) bottom crease (l) CC (m) unified

Figure 21: *Good and bad alignment of a T_1-gon with creases.*

from the affine invariance of the construction. By [GP15], isogeometric analysis (IgA) using the surface as physical domain requires functions with the same geometric continuity as the surface. While for geometry some degrees of freedom are sacrificed to obtain better shape, IgA uses the maximal set of basis functions of a fixed smoothness class. This is the same set that is considered for refinability. The following exhibits these τ-functions and their refinements.

- (3, 5): For the default construction the tensor-border in Fig. 8a defines the gray-underlaid strips of BB-coefficients in Fig. 9b and Fig. 23a. The left and the right strips consist of jets $\mathbf{j}^1 \mathbf{q}^s$. By Lemma 5 the jets are nestedly refinable. The top and the bottom strips are refinable since they are obtained by degree-elevation. The 36 BB-coefficients marked as ○ in Fig. 23a have linearly in-
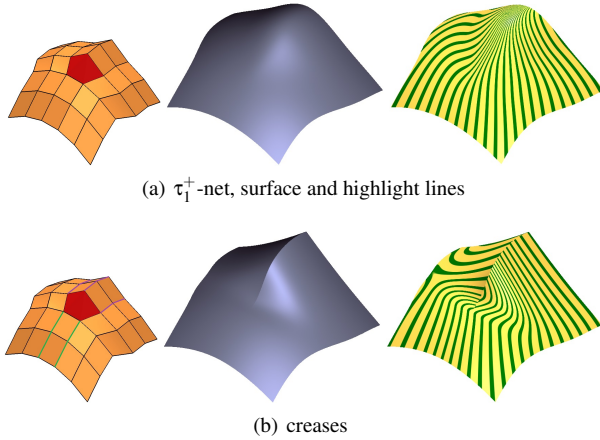
(a) τ_1^+-net, surface and highlight lines

(b) creases

Figure 22: *Introducing creases. (b) green layers delineate a double knot line behavior, and a triple knot line forms the top ridge.*

(a) $(3,5)$ (b) dofs   (c) refined dofs

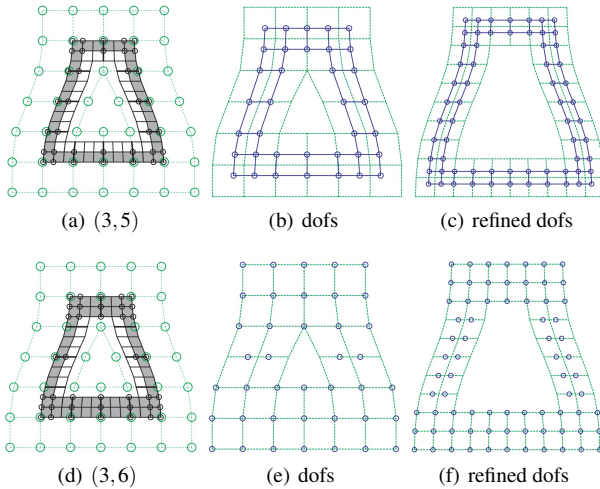(d) $(3,6)$ (e) dofs   (f) refined dofs

Figure 23: *Conversion and refinement. top: (a) unified net and BB-coefficients of the tensor border; (b) B-spline coefficients as dofs (blue disks); (c) refined dofs. bottom: same for degree (3,6).*

dependent generating functions; and are 1-1 with the 36 control points, marked as ∘ in Fig. 23b, of splines that are C^2 along the boundary frame and C^1 across. (Representation in B-spline form simplifies connection with the neighboring generating functions and reparameterization does not alter linear independence.) The ● in Fig. 9b are control points of a C^2/C^1 bi-degree $(3,5)$ spline cap. This yields a total of $42 + 36 = 78$ linearly independent functions. Fig. 23c and Fig. 9d show the refined sets of dofs.

- $(3,6)$: The dark-gray underlaid BB-coefficients in Fig. 11a correspond to 40 linearly independent functions whose BB-coefficients are shown in Fig. 23d, or, equivalently, to 40 B-spline control dofs in Fig. 23e. These are complemented by the 39 dofs marked ● in Fig. 11a; the refined sets of dofs is shown in Fig. 23f and Fig. 11b.

- $(3,9)$: In the curvature continuous case, all 42 input B-spline

control points define a linearly independent set of functions. They are complemented by 25 basis functions controlled by ● in Fig. 10.

Due to the present focus on geometry, we leave as future work the full characterization of how the dofs of the constructions interact within the global set of linearly independent functions on a heterogeneous mix of abutting T-nets, multi-sided configurations and B-splines.

6. Conclusion

The new unified construction is first in generating free-form surfaces with merging quad-strips of a quality suitable for automobile outer surfaces. Moreover, due to the unifying refinement, the construction is surprisingly local, requiring T_n-gons to only be surrounded by one layer of quads. This makes precise the notion of a *locally quad-dominant mesh*. In practice, this often averts global refinement to isolate irregularities which not only increases the patch count but can harm the overall shape.

The unified construction (of degree (3,5)) has two interesting variants: increasing the degree to (3,6) yields surfaces indistinguishable from curvature-continuous surfaces; and decreasing the degree to bi-3 yields surfaces whose jump in normal falls inside the range acceptable for automobile A-class design. The constructions are nestedly refinable and offer for engineering analysis linearly independent functions that form a partition of unity.

References

[ACSD*03] ALLIEZ P., COHEN-STEINER D., DEVILLERS O., LÉVY B., DESBRUN M.: Anisotropic polygonal remeshing. *ACM Tr Graph 22(3)* (2003), 485–493.

[ADS11] AUGSDÖRFER U. H., DODGSON N. A., SABIN M. A.: Artifact analysis on B-splines, box-splines and other surfaces defined by quadrilateral polyhedra. *Comp Aid Geom Design 28*, 3 (2011), 177–197.

[Aut19] AUTODESK: Tutorial at http://help.autodesk.com/view/alias/2015/enu/?guid=guid-2fce06eb-8ef7-4507-92f7-82a73a0df378, 2019. Apr07.

[BC94] BEIER K.-P., CHEN Y.: Highlight-line algorithm for realtime surface-quality assessment. *Comp-Aid Design 26*, 4 (1994), 268–277.

[BCE*13] BOMMES D., CAMPEN M., EBKE H.-C., ALLIEZ P., KOBBELT L.: Integer-grid maps for reliable quad meshing. *ACM Trans. Graph 32*, 4 (2013), 98:1–98:12.

[CADS09] CASHMAN T. J., AUGSDÖRFER U. H., DODGSON N. A., SABIN M. A.: NURBS with extraordinary points: high-degree, non-uniform, rational subdivision schemes. *ACM Tr Graph 28*, 3 (2009), 46:1–46:9.

[CC78] CATMULL E., CLARK J.: Recursively generated B-spline surfaces on arbitrary topological meshes. *Computer-Aided Design 10* (Sept. 1978), 350–355.

[CZ17] CAMPEN M., ZORIN D.: Similarity maps and field-guided T-splines: a perfect couple. *ACM Trans. Graph 36*, 4 (2017), 91:1–91:16.

[dB78] DE BOOR C.: *A Practical Guide to Splines*. Springer, 1978.

[DeR90] DEROSE T. D.: Necessary and sufficient conditions for tangent plane continuity of Bézier surfaces. *Comp Aid Geom Design 7*, 1 (1990), 165–179.

[Far88] FARIN G.: *Curves and Surfaces for Computer Aided Geometric Design: A Practical Guide*. Academic Press, 1988.

[GJS12] GIANNELLI C., JÜTTLER B., SPELEERS H.: THB-splines: The truncated basis for hierarchical splines. *Computer Aided Geometric Design 29*, 7 (2012), 485–498.

[GP15] GROISSER D., PETERS J.: Matched G^k-constructions always yield C^k-continuous isogeometric elements. *Computer Aided Geometric Design 34* (March 2015), 67–72.

[JTPSH15] JAKOB W., TARINI M., PANOZZO D., SORKINE-HORNUNG O.: Instant field-aligned meshes. *ACM Trans. Graph 34*, 6 (2015), 189.

[KBZ15] KOVACS D., BISCEGLIO J., ZORIN D.: Dyadic T-mesh subdivision. *ACM Trans. Graph. 34*, 4 (July 2015), 143:1–143:12.

[KNP07] KÄLBERER F., NIESER M., POLTHIER K.: Quadcover - surface parameterization using branched coverings. *Comput. Graph. Forum 26*, 3 (2007), 375–384.

[KP15] KARČIAUSKAS K., PETERS J.: Improved shape for multi-surface blends. *Graphical Models 8* (2 2015), 87–98.

[KP19a] KARČIAUSKAS K., PETERS J.: Localized G-splines for quad & T-gon meshes. In *Proc of GMP 2019* (Mar 2019), T Ju J Kosinka Y. L., (Ed.), pp. 1–10.

[KP19b] KARČIAUSKAS K., PETERS J.: Refinable smooth surfaces for locally quad-dominant meshes with T-gons. In *Proc of SMI 2019* (May 2019), Shape Modelling International 2019, pp. 1–10.

[KPP17] KARČIAUSKAS K., PANOZZO D., PETERS J.: T-junctions in spline surfaces. *ACM Tr on Graphics 36*, 5 (2017), 170:1–9.

[Kra98] KRAFT R.: *Adaptive und linear unabhängige Multilevel B-Splines und ihre Anwendungen*. PhD thesis, U of Stuttgart, 1998.

[KSD14] KOSINKA J., SABIN M. A., DODGSON N. A.: Subdivision surfaces with creases and truncated multiple knot lines. *Comput. Graph. Forum 33*, 1 (2014), 118–128.

[LKH08] LAI Y.-K., KOBBELT L., HU S.-M.: An incremental approach to feature aligned quad dominant remeshing. In *Symp Solid & Phys Modeling* (2008), Haines E., McGuire M., (Eds.), ACM, pp. 137–145.

[LS08] LOOP C. T., SCHAEFER S.: G ^{2} tensor product splines over extraordinary vertices. *Comput. Graph. Forum 27*, 5 (2008), 1373–1382.

[MPZ14] MYLES A., PIETRONI N., ZORIN D.: Robust field-aligned global parametrization. *ACM Trans. Graph. 33*, 4 (July 2014), 135:1–135:14.

[PBJW14] PENG C.-H., BARTON M., JIANG C., WONKA P.: Exploring quadrangulations. *ACM Trans. Graph 33*, 1 (2014), 12:1–12:13.

[RLL*06] RAY N., LI W.-C., LÉVY B., SHEFFER A., ALLIEZ P.: Periodic global parameterization. *ACM Tr Graph 25*, 4 (2006), 1460–1485.

[STJ*17] SCHERTLER N., TARINI M., JAKOB W., KAZHDAN M., GUMHOLD S., PANOZZO D.: Field-aligned online surface reconstruction. *ACM Trans. Graph 36*, 4 (2017), 77:1–77:13.

[SZBN03] SEDERBERG T. W., ZHENG J., BAKENOV A., NASRI A.: T-splines and T-NURCCs. In *Proc ACM SIGGRAPH* (2003), Hodgins J., Hart J. C., (Eds.), vol. 22(3) of *ACM Tr Graph*, pp. 477–484.

[WZLH17] WEI X., ZHANG Y. J., LIU L., HUGHES T. J. R.: Truncated T-splines: Fundamentals and methods. *Comp Meth Appl Mech Eng*, 316 (2017), 349–372.

[YZ04] YING L., ZORIN D.: A simple manifold-based construction of surfaces of arbitrary smoothness. *ACM Tr Graph 23*, 3 (2004), 271–275.

[ZSW10] ZADRAVEC M., SCHIFTNER A., WALLNER J.: Designing quad-dominant meshes with planar faces. *Comput. Graph. Forum 29*, 5 (2010), 1671–1679.

Appendix. τ_2-surfaces

Due to the change of density in two directions, τ_2-constructions differ from their τ_0- and τ_1-counterparts. Virtual refinement and reparameterization, the approach used in the unified construction, resulted in lower quality than the following τ_2-construction.
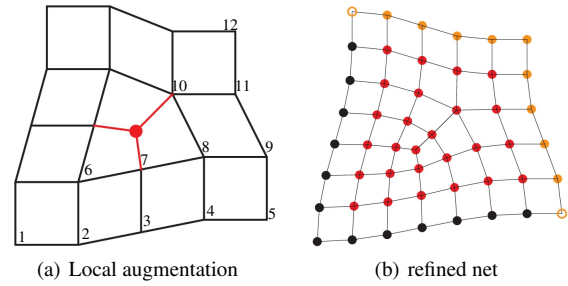

(a) Local augmentation (b) refined net

Figure 24: *T_2-configuration.*

– Define a new node • in Fig. 24a as a weighted sum of the initial nodes with the weights

1:6=	0.017	−0.017	0.023	−0.021	0.016	0.024
7:12=	0.201	0.231	−0.039	0.286	−0.069	0.023

(Due to diagonal symmetry of the construction only a subset of the weights are listed corresponding to the labels in Fig. 24a.)

– Connect • as shown in Fig. 24a.
– Apply one Catmull-Clark refinement step to the augmented net. This yields the new control points in Fig. 24b: • stem from the initial τ_2-net and • are influenced by the added control point. (The upper and right nodes depend on outside neighbors.)
– Apply a multi-sided hole filling construction to the net in Fig. 24b.

The last step could use, e.g. [LS08] or [YZ04], but applies [KP15], a low degree, refinable construction of good quality. Fig. 25 illustrates how the construction improves on its main alternatives: Catmull-Clark subdivision [CC78] (Fig. 25b, c) and [KPP17] (Fig. 25e, f).
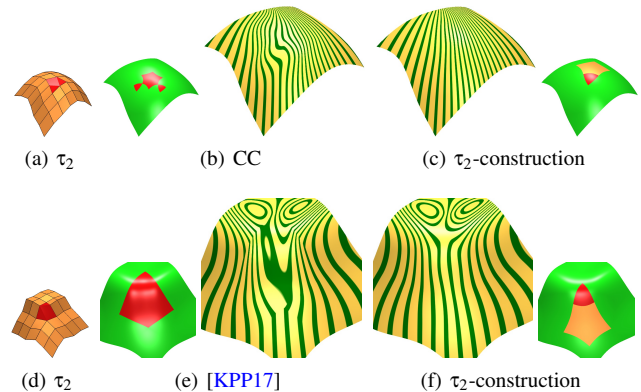

(a) τ_2 (b) CC (c) τ_2-construction

(d) τ_2 (e) [KPP17] (f) τ_2-construction

Figure 25: *τ_2-meshes. (a) convex, (d) creased. Comparison of the τ_2-construction with [KPP17] and Catmull-Clark subdivision (CC).*